Available online at www.sciencedirect.com
ScienceDirect
Infrared Physics & Technology 50 (2007) 149–155
INFRARED PHYSICS & TECHNOLOGY
www.elsevier.com/locate/infrared

Demonstration of 640 × 512 pixels long-wavelength infrared (LWIR) quantum dot infrared photodetector (QDIP) imaging focal plane array ☆

S.D. Gunapala [a,*], S.V. Bandara [a], C.J. Hill [a], D.Z. Ting [a], J.K. Liu [a], S.B. Rafol [b], E.R. Blazejewski [a], J.M. Mumolo [a], S.A. Keo [a], S. Krishna [c], Y.-C. Chang [a,1], C.A. Shott [d]

[a] The Jet Propulsion Laboratory, California Institute of Technology, 4800 Oak Grove Drive, Pasadena, CA 91109, United States
[b] The Infravision Systems, 2400 Lincoln Avenue, Altadena, CA 91001, United States
[c] University of New Mexico, 1313 Goddard Street SE, Albuquerque, NM 87106, United States
[d] The FLIR Systems Inc., Indigo Operations, 70 Castilian Dr., Goleta, CA 93117, United States

Available online 8 December 2006

Abstract

We have exploited the artificial atom-like properties of epitaxially grown self-assembled quantum dots (QDs) for the development of high operating temperature long wavelength infrared (LWIR) focal plane arrays (FPAs). QD infrared photodetectors (QDIPs) are expected to outperform quantum well infrared detectors (QWIPs) and are expected to offer significant advantages over II–VI material based FPAs. We have used molecular beam epitaxy (MBE) technology to grow multi-layer LWIR dot-in-a-well (DWELL) structures based on the InAs/InGaAs/GaAs material system. This hybrid quantum dot/quantum well device offers additional control in wavelength tuning via control of dot-size and/or quantum well sizes. DWELL QDIPs were also experimentally shown to absorb both 45° and normally incident light. Thus we have employed a reflection grating structure to further enhance the quantum efficiency. The most recent devices exhibit peak responsivity out to 8.1 μm. Peak detectivity of the 8.1 μm devices has reached $\sim 1 \times 10^{10}$ Jones at 77 K. Furthermore, we have fabricated the first long-wavelength 640 × 512 pixels QDIP imaging FPA. This QDIP FPA has produced excellent infrared imagery with noise equivalent temperature difference of 40 mK at 60 K operating temperature.

1. Introduction

The artificial atom-like properties of epitaxially self-assembled quantum dots (QDs) were exploited in this work for the development of high operating temperature long wavelength infrared (LWIR) focal plane arrays (FPAs). QDs are nanometer-scale islands that form spontaneously on a semiconductor substrate due to lattice mismatch. QDIPs are expected to have significant advantages over quantum well infrared detectors (QWIPs) [1–8]. QD infrared photodetectors (QDIPs) are fabricated using robust wide band gap III–V materials which are well suited to the production of highly uniform LWIR arrays. QD based infrared photodetectors have the potential to make a significant impact on the next generation of infrared imaging systems. QDIPs possess all of the advantages of traditional III–V based infrared photodetectors, such as: extremely high operability, mature fabrication technology, very large formats, and material production that is increasingly high volume and low cost. The addition of active nanoscale particles (i.e. QDs) embedded within the III–V infrared detector allows for higher operating temperatures and increased band gap tunability without sacrificing the economic advantages of the mature III–V infrared imaging system pipeline.

☆ The research described in this paper was performed by the Jet Propulsion Laboratory, California Institute of Technology.

* Corresponding author.
E-mail address: sarath.d.gunapala@jpl.nasa.gov (S.D. Gunapala).
[1] Permanent address: Department of Physics, University of Illinois at Urbana-Champaign, Urbana, IL 61801, United States.

1350-4495/$ - see front matter © 2006 Elsevier B.V. All rights reserved.
doi:10.1016/j.infrared.2006.10.004

The 3D confinement of the nanoscale QDs enables normal incidence absorption by modifying the optical transition selection rule and increases the photo-excited carrier lifetime by reducing optical phonon scattering via the "phonon bottleneck" mechanism. The former enhances quantum efficiency, while the latter raises operating temperature. Consequently, QDIPs offer increased performance over existing QWIP FPAs. Thus the thrust of this work has been to further uncover and manipulate the properties of QDs and to devise device and optical enhancement structures in order to exceed the performance and/or temperature of operation of quantum well based infrared arrays.

2. The dot-in-the-well infrared photodetector

The main benefit in using the QD approach stems from 3D quantum confinement, which (1) enables normal incidence absorption by modifying the optical transition selection rule, and, (2) increases the photo-excited carrier lifetime by reducing optical phonon scattering via the "phonon bottleneck" mechanism [1–6]. However, QDs also have some drawbacks that need to be addressed. In a typical detector structure, QD densities are low (compared to the number of dopants in the active regions of QWIPs); so while individual QDs are efficient absorbers, typical QD densities are not high enough to achieve high quantum efficiency. Thus, while QD based infrared detectors have clearly demonstrated normal incidence absorption [5,6], and, in some instances, higher operating temperature as well [5–12], they are still lacking in quantum efficiency and responsivity.

The first-generation QDIPs are high-gain, low-quantum-efficiency devices. Improving quantum efficiency is a key to achieving a competitive QD-based FPA technology. This can be accomplished by increasing the QD density, or by enhancing the infrared absorption in the QD-containing material. There are various versions of QDIPs, based on different materials and designs. After considering all types of competing QD-based approaches, we feel that one of the most promising options for LWIR FPAs is the use of the dot-in-a-well (DWELL) QDIP [10,11,13]. Our specific implementation uses InAs and InGaAs QDs embedded in GaAs/AlGaAs multi-quantum well structures, as illustrated in Fig. 1. This material system can sustain a large number of QD stacks without suffering material degradation, thereby allowing high dot density. The host GaAs/AlGaAs multi-quantum well structures are highly compatible with the mature FPA fabrication process that we use routinely to make QWIP FPAs; in that sense, this system may be viewed as simply a QWIP with embedded InAs QDs. Similar to other intersubband detectors, DWELLs operate by the photoexcitation of electrons between energy levels in the potential well created by the nano-scale QD in a well structure. The right panel of Fig. 1 shows that, under an applied bias voltage, these photo-excited carriers can escape from the potential wells and be collected as photocurrent. The wavelengths of the spectral peaks (λ_p) are determined by the energy difference between quantized states in the DWELL. The hybrid quantum-dot/quantum-well, or dot-in-a-well (DWELL), device offers two advantages: (1) challenges in wavelength tuning through dot-size control can be compensated in part by engineering the quantum well sizes, which can be controlled precisely; (2) quantum wells can trap electrons and aid in carrier capture by QDs, thereby facilitating ground state refilling.

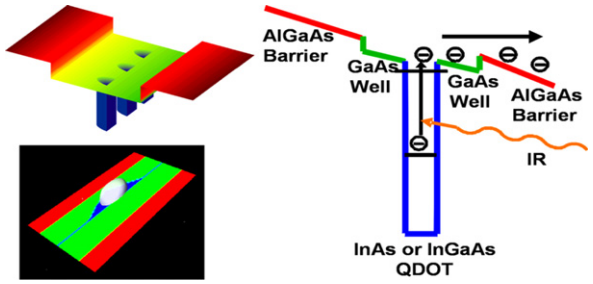

Fig. 1. Illustration of the dot-in-a-well (DWELL) device. Top left panel shows the potential profile, with three pyramid shaped dots embedded in the quantum well. The bottom left panel displays a calculated DWELL ground state wave function, represented by a white translucent equal-probability isosurface, localized by a pyramidal quantum dot. The right panel illustrates the operation of a DWELL infrared detector.

3. Quantum dot material growth

QDs can be fabricated by taking advantage of a strain-induced transformation that happens naturally in the initial stages of epitaxial growth for lattice-mismatched materials. One highly successful method of achieving QDs is through self-organized growth in the Stranski–Krastanow growth mode [14]. Similar to quantum wells, these structures are fabricated by MOCVD or MBE using III–V materials (e.g. InGaAs/AlAs/GaAs/InAs). 3D islands can be formed spontaneously during strained layer epitaxy, and they exhibit good uniformity in size, shape and spatial distribution. By using a smaller band gap material for the strained layer (InAs) and a larger band gap material for the barrier (GaAs or AlGaAs), three-dimensional confinement can be achieved. The QD island dimensions are controllable by changing growth conditions. Our MBE chamber is equipped with dual Ga, In, and Al cells for flux of the group III elements, and a valved cracking As source for the group V. In addition to standard III–V dopants (Be, Si, Te), the chamber is also equipped with a valved cracking source for Sb, allowing for the incorporation of more esoteric InSb QDs or AlSb anti-dots as well as a nitrogen plasma source for countering the tensile strain of InGaAs wells with nitrogen incorporation. The substrate temperature and all cell temperatures are fully computer controlled to meet the rigorous temperature cycling demands of high-quality DWELL QDIP growth. The chamber is also used for the production of large format Ga(In)As/AlGaAs FPAs, and has demonstrated excellent uniformity for wafer sizes up to 100 mm (4 in.). Relaxation-free growth of over

30 periods, twice as many as reported for conventional DWELL [10,13] structures has achieved by lowering the indium content of the InGaAs wells. Full use of our closed-loop detector development cycle, including feedback from photoluminescence, AFM and X-ray measurements, was necessary to ensure that the quantum efficiency of the overall structure increased along with stack number. This has led to much higher quantum efficiency in our structures than previously reported values for DWELL QDIP structures [10].

4. Test detector fabrication

All DWELL-QDIP wafers were grown on semi-insulating 4 in. GaAs substrates using a Veeco Gen-III MBE Reactor. After evaluating material quality, selected wafers were processed into test detector mesas. After the 200 μm × 200 μm square mesas are defined by lithography, the DWELL-QDIP test detectors were fabricated by standard wet and dry chemical etching through the stack of photosensitive layers into the doped GaAs bottom contact layer. The top contact of the detectors were covered with Au/Ge and Au for an Ohmic contact which also serves as a reflector for light incident through the bottom contact, allowing two passes through the active layers.

Initial QDIP characterization of discrete devices included measurements of the room-temperature absorption spectra, side [15,16] and normal incident responsivity spectra, dark current, and noise. These detectors were tested in a cryogenically cooled test bed using a calibrated blackbody source to evaluate responsivity of the detector over the relevant range of operating temperatures and bias voltages. The test results were used to verify and adjust the model used in designing the material parameters. This cycle was iterated several times in order to develop the recipe for the final optimized detector wafer used to make FPAs.

5. DWELL QDIP absorption quantum efficiency

A separate 8-pass polished waveguide structure was fabricated for absorption measurements [15,16]. Fig. 2 shows the measured absorption QE from a 30-stack DWELL QDIP, with a peak value at approximately 2.7%. To our knowledge, this is the best measured intrinsic absorption QE to date in a QD based LWIR infrared detector. During this development we have measured the normal and 45° incidence responsivity of DWELL QDIP samples. A typical set of results is shown in Fig. 3. As hoped, the normal incidence responsivity (relative to the 45° responsivity) is much stronger (almost 1 order of magnitude) than that found in a typical QWIP. At the same time, we also find that the 45° incidence responsivity is 4–5 time stronger than the normal incidence responsivity. This implies that at these wavelengths, the DWELL QWIPs not only have good absorption for normal incidence (x, y-polarized; with z-being the normal incidence direction) light, it also

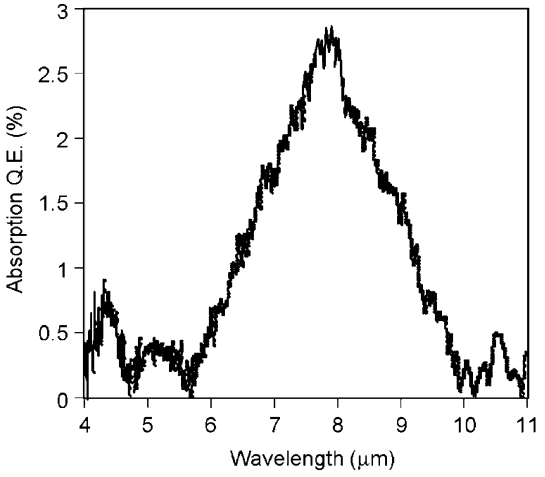

Fig. 2. The measured internal absorption quantum efficiency (no grating or cavity effects) for a 30-stack DWELL QDIP.

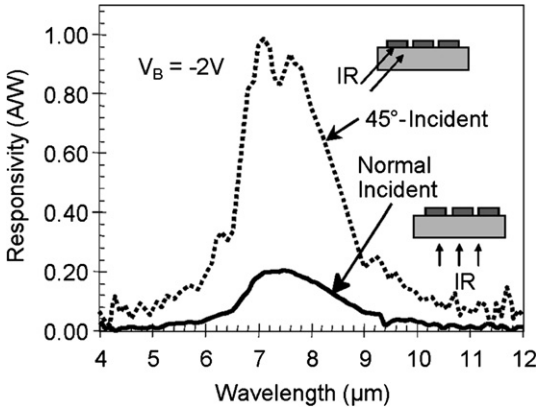

Fig. 3. DWELL QDIP spectral responsivity measured for (a) normal incidence, (b) 45° incidence.

absorbs inclined (or side) incidence (z-polarized) light even more strongly [9]. This knowledge has prompted an important design modification, as we now wish to take advantage of the DWELL QDIP's ability to absorb both normal and inclined incidence light in order to maximize quantum efficiency. As in QWIPs, normal incidence light can be coupled to the z-polarization light absorption mechanism in DWELL QDIPs by using a reflection grating. Due to our extensive experience in designing and fabricating FPA-compatible integrated optical structures for QWIPs, we were in an excellent position to implement the grating reflector enhanced QDIP. Fig. 4 shows our preliminary experimental results on grating enhancement. Normal incidence responsivity was measured for a DWELL QDIP sample, fabricated both with and without a reflection grating. It should be noted here that the substrate was not thinned in either case, hence resonant grating cavity effects have not been incorporated. Nevertheless, the device with the reflection grating shows approximately three times larger normal incident responsivity than the one without, clearly indicating the promise of this approach.

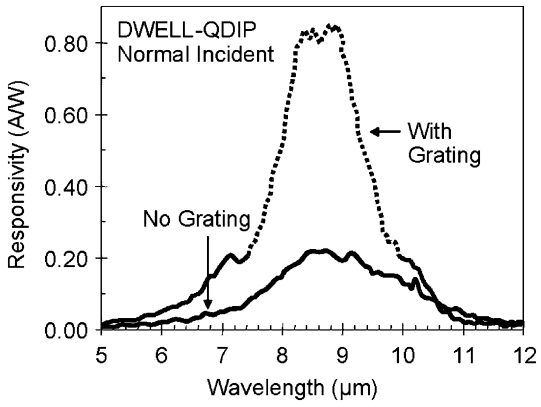

Fig. 4. Normal incidence spectral responsivity of a DWELL-QDIP with and without reflection gratings.

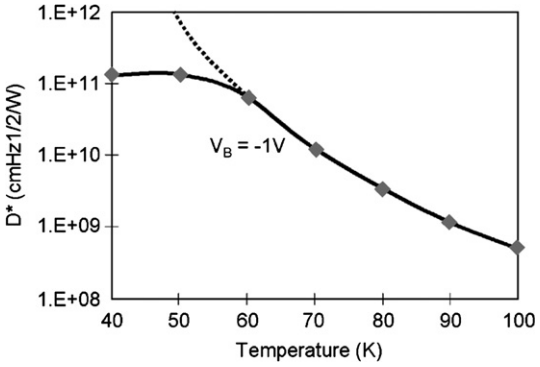

Fig. 6. Dark current limited and background (300 K, *f*/2 optics) limited specific detectivity of DWELL-QDIP as a function of operating temperature. Detectivities are calculated using experimentally measured spectral responsivity, dark current, and photoconductive gain of the detector.

Given that the gain of DWELL QDIPs is quite different from other intersubband detectors, it is worthwhile to examine how this affects the detector performance. Sensitivity of DWELL QDIPs can be evaluated by measuring parameters such as absolute spectral responsitivity $R(\lambda)$, absorption quantum efficiency (internal) η, photocurrent (I_P), dark current I_D, noise current i_n, and specific detectivity (D^*). Similar to other intersubband photodetectors, these parameters are linked each other through the photoconductive gain (g) of the detector, $R = e\eta g/(hc/\lambda)$, $i_n = \sqrt{4e(I_D + I_P)g\Delta f}$, and $D^* = R\sqrt{A\Delta f}/i_n$ [15,16].

Here, e is the electron charge, Δf is the bandwidth, A is the detector area, and hc/λ is the photoexcitation energy. When the detector operates in background limited conditions ($I_P \gg I_D$), since I_P is proportional to gain, D^* depends only on the absorption quantum efficiency η, regardless of the size of the photoconductive gain. Therefore, improving absorption quantum efficiency is the key to improving the ultimate performance of these detectors [15,16]. Fig. 5 shows the dark current as a function of temperature at various operating bias conditions. Fig. 6 shows D^* of this detector as a function of device temperature at operating bias $V_B = -1$ V. This figure shows that the DWELL detector reaching background limited $D^* \sim 1 \times 10^{11}$ Jones around $T = 50$ K temperature. We expect to improve D^* through reduction of dark current and increase in quantum efficiency. Specifically, (1) dark current reduction would extend the plateau of the BLIP (background limited performance) D^* curve to higher temperature, (2) quantum efficiency increase would shift the BLIP D^* curve upward over the entire temperature range. Further reduction in dark current would help to achieve BLIP performance at higher operating temperatures.

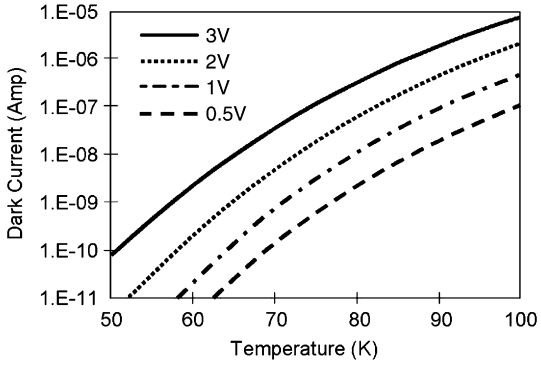

Fig. 5. Dark current vs. operating temperature curves of a DWELL QDIP detector at various device bias conditions. The device area is 25×25 μm^2.

6. Focal plane array fabrication

After establishing optimized layer thickness and growth conditions for the LWIR DWELL-QDIP, the FPA development effort began with the growth of wafers on 3 in. semi-insulating GaAs substrates. Selected wafers were processed into FPAs. We regularly use established III–V material fabrication processes to develop QWIP FPAs including complicated multilevel structures and very-large-formats. These procedures are directly applicable for QD-based devices due to the similarity of the underlying material systems. These processes (including grating fabrication, detector pixel isolation, metal evaporation, metal lift-off and Ohmic contact annealing) are carried out at the wafer level (see Fig. 7). Generally, an optical coupling grating requires high resolution photolithographic techniques to meet critical dimensions in the grating pattern. Photolithography was performed with a Cannon Stepper, which maintains the large format array uniformity across the entire wafer while minimizing defects during lithography throughout the processing cycles. In preparation for hybridization, In-bumps are evaporated in each pixel of the entire wafer and each detector array is diced for hybridization with an ISC-9803 read out integrated circuit (ROIC). In bump-evaporation and hybridization procedures were carried out at FLIR Indigo Systems.

After the 640×512 pixel QDIP detector arrays were hybridized to a 640×512 pixel ROIC, a simple electronic functionality test was performed to evaluate the FPAs. Then we thinned the selected FPA hybrids by removing the entire substrate while leaving the detector pixels, the

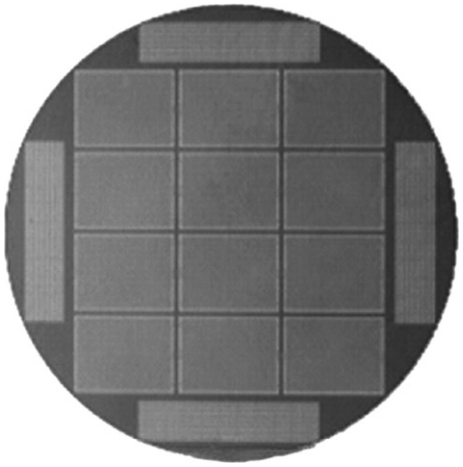

Fig. 7. A 3-in. GaAs wafer with twelve 640×512 pixels QDIP FPAs.

bottom contact layer and the dielectric mirror. During thinning, the entire substrate material was removed by abrasive polishing, wet chemical etching followed by dry etching that ends at the epitaxially grown selective etch layer. This thinned detector array completely eliminates the thermal mismatch issue between the CMOS ROIC and the GaAs/InAs/AlAs based detector array, pixel outages, and pixel-to-pixel optical cross talk of the FPA. Basically, the thinned GaAs based QDIP FPA membrane adapts to the thermal expansion and contraction coefficients of the silicon readout multiplexer. Thus, thinning has played an extremely important role in the fabrication of large area FPA hybrids. Elimination of thermal mismatch is a process of paramount importance in achieving high-quality, large area arrays without pixel delamination [15]. Typically, twelve 640×512 detector arrays can be processed from a single 3 in. GaAs wafer (see Fig. 7).

7. Focal plane array demonstration

Selected detector hybrids were mounted and wire-bonded to a leadless chip carrier (LCC). A specially designed dewar was used to characterize the FPA functionality using a general-purpose electronic system from SE-IR Incorporated. The SE-IR system was programmed to generate complex timing patterns, and was reconfigured to handle a development grade FPAs. The best performance was determined by optimizing operating-parameters for each FPA. The FPAs were characterized for pixel responsivity, quantum efficiency, noise, D^*, NEΔT, pixel operability, before and after correction uniformity (contribution form both spatial and temporal), and pixel operability. The spectral responsivity of the FPA was determined using a separate single mesa processed with the FPA. NEΔT as a function of bias and integration time at a fixed operating temperature was used as a metric for parameter optimization.

Since the QDIP is a high impedance device at operating temperature, it should yield a very high charge injection coupling efficiency into the integration capacitor of the multiplexer. Charge injection efficiency can be obtained from $E_{\text{inj}} = g_{\text{m}} R_{\text{D}}/(1 + g_{\text{m}} R_{\text{D}})$, where g_{m} is the transconductance of the MOSFET and is given by $g_{\text{m}} = eI_{\text{Det}}/kT$. The differential resistance R_{Det} of the $23 \times 23\ \mu\text{m}^2$ pixels at -350 mV bias is $5.5 \times 10^{10}\ \Omega$ at $T = 60$ K and detector capacitance C_{Det} is 1.4×10^{-14} F. The detector total current is $I_{\text{Det}} = 17$ pA under the same operating conditions. However, the dynamic resistance of the detector and ROIC is given by $R_{\text{D}}.C_{\text{ROIC}} = t_{\text{int}}$, where C_{ROIC} is the capacitance of the ROIC integration capacitor and t_{int} is the integration time. We have integrated the signal for 20 ms. The input capacitance of ISC 9803 ROIC is 350 fF, which yields R_{D} of $5.7 \times 10^{10}\ \Omega$. According to the equation above, the charge injection efficiency $E_{\text{inj}} = 99.65\%$ at a frame rate of 50 Hz. The FPA was back-illuminated through the flat thinned substrate membrane (thickness ≈1000 Å). This initial array gave very good images with >99% of the pixels working, demonstrating the high yield of GaAs technology. The operability was defined as the percentage of pixels having NEΔT within 2σ at 300 K background with $f/2$ optics and in this case operability happens to be equal to the pixel yield.

We have used the following equation to calculate the NEΔT of the FPA. $\text{NE}\Delta\text{T} = \sqrt{AB}/[D^*_{\text{B}}(\text{d}P_{\text{B}}/\text{d}T)\sin^2(\theta/2)]$, where D^*_{B} is the blackbody detectivity, $(\text{d}P_{\text{B}}/\text{d}T)$ is the derivative of the integrated blackbody power with respect to temperature, and θ is the field of view angle [i.e., $\sin^2(\theta/2) = (4f^2 + 1)^{-1}$, where f is the f number of the optical system]. The background temperature $T_{\text{B}} = 300$ K, the area of the pixel $A = (23\ \mu\text{m})^2$, the f number of the optical system is 2.3, and the frame rate is 30 Hz. Fig. 8 shows the experimentally measured NEΔT histogram of the FPA at an operating temperature of $T = 60$ K, bias $V_{\text{B}} = -350$ mV at 300 K background with $f/2$ optics. The mean NEΔT value is 40 mK. This agrees reasonably well with our estimated value of 25 mK based on test structure data. The read noise

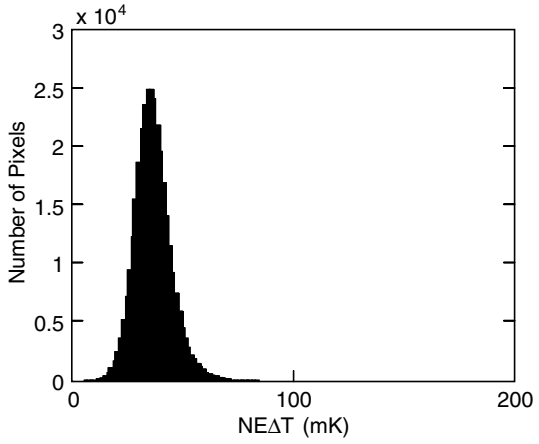

Fig. 8. Noise equivalent temperature difference (NEΔT) histogram of the 311,040 pixels of the 640×512 pixel QDIP FPA showing a high uniformity of the FPA. The non-uniformity (= standard deviation/mean) of this unoptimized FPA is only 0.2%.

of the multiplexer is 500 electrons. The experimentally measured peak quantum efficiency of the FPA was 5.0% (see Fig. 9). Thus, the quantum efficiency of the DWELL QDIP discussed in this paper has enhanced by a factor of 1.8 due to the resonant grating cavity. Similar grating cavity enhancement effects were observed in QWIP FPAs as well.

8. Focal plane array camera

A 640×512 pixel QDIP FPA hybrid was mounted onto a 84-pin LCC and installed into a laboratory dewar which is cooled by liquid nitrogen to demonstrate a LWIR imaging camera. The FPA was cooled to 60 K by pumping on liquid nitrogen and the temperature was stabilized by regulating the pressure of gaseous nitrogen. The other element of the camera is a 100 mm focal length AR coated germanium lens, which gives a $7.3° \times 5.9°$ field of view. It is designed to be transparent in the 8–12 μm wavelength range to be compatible with the QDIP's 8–9 μm operation. The digital data acquisition resolution of the camera is 14-bits, which determines the instantaneous dynamic range of the camera (i.e., 16,384) [15,16].

The measured mean NEΔT of the QDIP camera is 40 mK at an operating temperature of $T = 60$ K and bias $V_B = -350$ mV at 300 K background with $f/2$ optics. This is in good agreement with expected FPA sensitivity due to the practical limitations on charge handling capacity of the multiplexer, read noise, bias voltage and operating temperature. The uncorrected NEΔT non-uniformity of the 640×512 pixels FPA is about 3% (= sigma/mean). Fig. 8 shows the NEΔT histogram of this first unoptimized 640×512 pixel QDIP FPA and the higher sigma/mean was due to the reduced number of samples acquired during the measurement. The non-uniformity after two-point (17 °C and 27 °C) correction improves to less than 0.2%.

Video images were taken at a frame rate of 50 Hz at temperatures as high as $T = 60$ K using a ROIC capacitor having a charge capacity of 11×10^6 electrons (the maximum number of photoelectrons and dark electrons that can be counted in the integration time of each detector pixel). Fig. 10 shows an image taken with this long-wavelength 640×512 pixels QDIP camera.

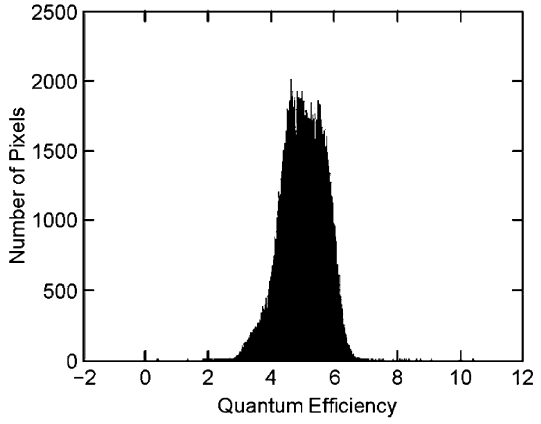

Fig. 9. Quantum efficiency histogram of the 311,040 pixels of the 640×512 pixel QDIP FPA.

Fig. 10. An image taken with the first 640×512 pixels QDIP LWIR focal plane array camera.

9. Conclusion

The goal of our development was to continually increase the D^* of the DWELL QDIP by maximizing quantum efficiency and responsivity while minimizing dark current. Our strategy has been to perform a survey of a wide range of techniques to identify the key issues for detector optimization. These include: material development for increasing the number of QD stacks, spacer/barrier layer for dark current blocking, variations in well structure for wavelength control, design of DWELL quasi-bound excited states, and QD size distribution control. All of these techniques have resulted in performance improvements, and all of them still have room for further improvement. This development effort has led to the best LWIR DWELL QDIP performance to date, and will provide the empirical basis for what will lead to our achieving the very ambitious sensitivity goals demanded by space-born imaging programs. In conclusion, we have demonstrated the first 640×512 pixel LWIR QDIP FPA with NEΔT of 40 mK at an operating temperature of 60 K.

Finally, it should be noted that in addition to the performance already discussed in this paper, the QDIP array technology offers additional positive attributes that should not be overlooked. Large substrates (6 in. wafers) are readily available for growth. A 6 in. GaAs wafer provides sufficient real estate to produce over forty 640×512 arrays at a 25 μm pitch. Since the QDIP arrays are thinned down to a membrane, indium bump hybrids can be quite large since the thermal mismatch issues between detector array and silicon are eliminated. Consequently, the QDIP interconnect operability is quite high. The smaller absorption volume of the QDIP structures indicates that their radiation hardness will be higher than the conventional QWIP devices. QWIP-like structures have been shown to exhibit very low $1/f$ noise. The lack of $1/f$ noise above 10 mHz

allows for stable calibrated staring and slow scan strategies commonly required in space-born applications. Of particular interest is the role that other FPA parameters such as operability and uniformity play in the quality of an image from a FPA. A more detailed discussion on this subject can be found elsewhere [16]. This treatment makes a significant point that when $D^* \geqslant 10^{10}$ cm $\sqrt{}$Hz/W, the FPA performance is limited by array uniformity and thus essentially independent of the detectivity. This attribute has been demonstrated in the high-quality images with low NEΔT taken by JPL's highly uniform QWIP FPAs.

Acknowledgements

We are grateful to R. Cox, S. Forouhar, P. Grunthaner, J. Hong, J. Hyon, C. Khan, K. Koliwad, T. Krabach, A. Larson, T. Luchik, R. Odle, C. Ruoff, R. Staehle, and N. Toomarian for encouragement and support during the development and optimization of QDIP FPAs at the Jet Propulsion Laboratory (JPL) for various applications. The authors would like to give their special thanks to Prof. Pallab Bhattacharya of the University of Michigan for his support during the early days of this work at JPL.

References

[1] V. Ryzhii, The theory of quantum-dot infrared photodetector, Semicond. Sci. Technol. 11 (1996) 759–765.
[2] J. Phillips, K. Kamath, P. Bhattacharya, Far-infrared photoconductivity in delf-organized InAs quantum dots, Appl. Phys. Lett. 72 (1998) 2020–2022.
[3] D. Pal, L. Chen, E. Towe, Intersublevel photoresponse of (InGa)As/GaAs quantum-dot photodetectors: Polarization and temperature dependence, Appl. Phys. Lett. 83 (2003) 4634–4636.
[4] S. Chakrabarti, A.D. Stiff-Roberts, P. Bhattacharya, S. Gunapala, S. Bandara, S.B. Rafol, S.W. Kennerly, High-temperature operation of InAs–GaAs quantum-dot infrared photodetectors with large responsivity and detectivity, IEEE Photonic. Tech. Lett. 16 (2004) 1361–1363.
[5] E.T. Kim, A. Madhukar, Z. Ye, J.C. Campbell, High detectivity InAs quantum dot infrared photodetectors, Appl. Phys. Lett. 84 (2004) 3277–3279.
[6] Z. Ye, J. Campbell, Z. Chen, E.T. Kim, A. Madhukar, Noise and photoconductive gain in InAs quantum-dot infrared photodetectors, Appl. Phys. Lett. 83 (2003) 1234–1236.
[7] P. Bhattacharya, X.H. Su, S. Chakrabarti, G. Ariyawansa, A.G.U. Perera, Characteristics of a tunneling quantum-dot infrared photodetector operating at room temperature, Appl. Phys. Lett. 86 (2005) 191106–191108.
[8] W. Zhang, H. Lim, M. Taguchi, S. Tsao, B. Movaghar, M. Razeghi, High-detectivity InAs quantum-dot infrared photodetectors grown on InP by metal-organic chemical-vapor deposition, Appl. Phys. Lett. 86 (2005) 191103–191104.
[9] V.G. Stoleru, E. Towe, Oscillator strength for interband transitions in (InGa)As/GaAs quantum dots, Appl. Phys. Lett. 83 (2003) 5026–5028.
[10] S. Krishna, Quantum dots-in-a-well infrared photodetector, J. Phys. D 38 (2005) 2142–2150.
[11] S. Raghavan, P. Rotella, A. Stintz, B. Fuchs, S. Krishna, C. Morath, D.A. Cardimona, S.W. Kennerly, High-responsivity, normal incidence long-wave infrared ($\lambda \sim 7.2$ μm) InAs/In0.15Ga0.85 dots-in-a-well detector, Appl. Phys. Lett. 81 (2002) 1369–1371.
[12] J. Jiang, K. Mi, S. Tsao, W. Zhang, H. Lim, T. O'Sullivan, T. Sills, M. Razeghi, G.J. Brown, M.Z. Tidrow, Demonstration of a 256×256 middle-wavelength infrared focal plane array based on InGaAs/InGaP quantum dot infrared photodetectors, Appl. Phys. Lett. 84 (2004) 2232–2234.
[13] S. Krishna, D. Forman, S. Annamalai, P. Dowd, P. Varangis, T. Tumolillo, A. Gray, J. Zilko, K. Son, M. Liu, J. Campbell, D. Carothers, Demonstration of a 320×256 two-color focal plane array using InAs/InGaAs quantum dots in well detector, Appl. Phys. Lett. 86 (2005) 193501–193503.
[14] I.N. Stranski, L. Krastanow, Zur Theorie der orientierten Ausscheidung von Ionenkristallen aufeinander, Sitzungsberichte d. Akad. D. Wissenschaften in Wien Mathnaturwiss 146 (1937) 797–810.
[15] S.D. Gunapala, S.V. Bandara, J.K. Liu, E.M. Luong, S.B. Rafol, J.M. Mumolo, D.Z. Ting, J.J. Bock, M.E. Ressler, M.W. Werner, P.D. LeVan, R. Chehayeb, C.A. Kukkonen, M. Levy, P. LeVan, M.A. Fauci, Quantum well infrared photodetector research and development at jet propulsion laboratory, Sensors Mater. 12 (2000) 327–351.
[16] S.D. Gunapala, S.V. Bandara, Quantum Well Infrared Photodetector (QWIP) Focal Plane ArraysSemiconductors and Semimetals, 62, Academic Press, 1999, pp. 197–282.